Journal of Materials Chemistry C

ROYAL SOCIETY OF CHEMISTRY

PAPER

View Article Online
View Journal | View Issue

Cite this: J. Mater. Chem. C, 2025, 13, 5017

Luminescent lanthanide complexes supported by ditopic Schiff-base/calix[4]arene macrocycles: synthesis, structure, and luminescence properties of $[Ln_2(H_2L^2)(H_2O)_2]$ (Ln = La, Eu, Tb, Yb)†

Christian Zocher, ‡[a] Josef Taut, ‡[a] Christian Laube, [bc] Martin Börner,[a] Patrick Melix, [d] Steve Ullmann,[e] Bernd Abel, [c] Ralf Tonner-Zech [d] and Berthold Kersting *[a]

The ditopic macrocycle H_8L^2 comprising two 3,3′-dihydroxy-4,4′-bis(iminomethyl)-biphenyl and two calix[4]arene units was synthesized and its ability to bind lanthanide ions has been studied. H_8L^2 reacts readily with Ln(III) nitrate salts in the presence of NEt_3 to support dinuclear neutral complexes of composition $[Ln_2(H_2L^2)(H_2O)_2]$ (Ln = La^{3+} (**1**), Eu^{3+} (**2**), Tb^{3+} (**3**), and Yb^{3+} (**4**)). The crystal structure of the ditopic calix[4]arene ligand reveals a centrosymmetric molecule with an overall "S-shape" structure and a cone-conformation. The molecular structure of the Yb complex **4** is also "S-shape" indicative of some degree of preorganization imposed by the ligand constraints. The Yb^{3+} ions are seven-coordinated (distorted monocapped trigonal prismatic coordination environment (NO_6 donor set)). DFT calculations for the La complex **1** (at the r^{2}SCAN-3c level of computation) implies an isostructural series of compounds. The ligand and complexes exhibit strong absorptions ($\varepsilon > 10^4$ M^{-1} cm^{-1}) in the 250–440 nm range attributed to ligand-based π–π* and n–π* transitions. The bis(iminomethyl)biphenyl linkers were found to sensitize Eu^{III} and Tb^{III} emission (λ_{ex} = 370 nm and 405 nm) in the solid state at 295 K. A material containing statistically distributed Tb^{III} and Eu^{III} ions reveals upon 370 nm excitation only Eu^{3+} emission lines indicative of intermolecular energy transfer processes between the Ln^{3+} ions.

Received 14th October 2024,
Accepted 13th January 2025

DOI: 10.1039/d4tc04407j

rsc.li/materials-c

Introduction

Luminescent materials based on Ln^{3+} ions are of interest due to their unique photophysical properties that make them suitable for a range of potential applications such as optical imaging, bioprobes, sensors, visible emitters for display, solar energy conversion, and lighting technology, near-infrared (NIR) emitters for lasers, optical fibers and amplifiers to name but a few.[1–6] Much attention is currently focused on the development and study of well-defined lanthanide compounds containing two or more different Ln(III) ions.[7–14] A number of classes of heterolanthanide assemblies have been described, such as multidimensional coordination frameworks, discrete molecules, and flexible large molecules formed by two or more coordinating units connected by a linker.[15,16] The combination of different lanthanide complexes in polymeric structures, for example, enables the simultaneous emission of different lanthanide ions upon single-wavelength excitation.[16,17] There is a wide range of color shade accessible from red to green[18–22] and from blue to green[20] in Tb/Eu mixed complexes. Besides these shifts it is also possible to force an energy transfer between two or more lanthanide ions as observed for *e.g.* in Y/Tb,[23] Sm/Tb,[24] and Tb/Eu[22,25–29] complexes. The understanding and control of the luminescent properties by effective sensitization is extremely important particularly in sensory applications or in light-emitting diodes (LED) technology.[30]

The synthesis of discrete, bimetallic lanthanide complexes can be accomplished by using multidentate ligand systems that allow juxtaposition of the Ln^{3+} ions in a stable and rigid coordination environment.[31] Functionalized calix[4]arenes[32–34] have turned out to be a class of versatile supporting ligands for a number of stable lanthanide complexes.[35–42] Several calixarenes

[a] Institut für Anorganische Chemie, Universität Leipzig, Johannisallee 29, D-04103 Leipzig, Germany. E-mail: b.kersting@uni-leipzig.de; Fax: +49(0)341-97-36199
[b] Leibniz-Institut für Oberflächenmodifizierung e.V., Permoserstraße 15, D-04318 Leipzig, Germany
[c] Institut für Technische Chemie, Universität Leipzig, Linnéstraße 3-5, D-04103 Leipzig, Germany
[d] Wilhelm-Ostwald-Institut für Physikalische und Theoretische Chemie, Universität Leipzig, Johannisallee 29, D-04103 Leipzig, Germany
[e] Institut für Nichtklassische Chemie e.V., Universität Leipzig, Permoserstraße 15, D-04318 Leipzig, Germany

† CCDC 2384275, 2384276 and 2410730. For crystallographic data in CIF or other electronic format see DOI: https://doi.org/10.1039/d4tc04407j

‡ These authors contributed equally to this work.

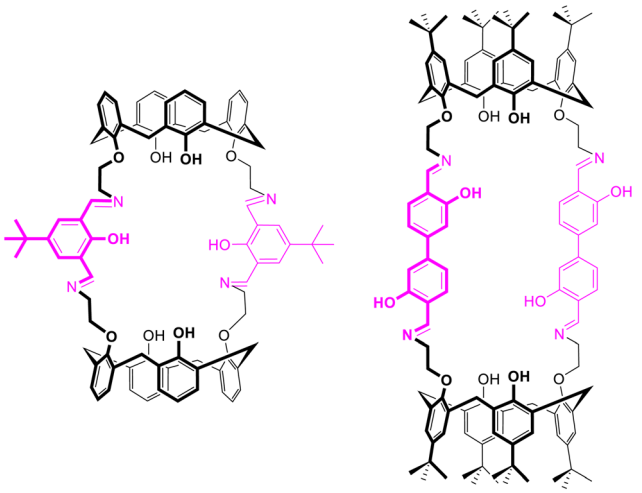

Fig. 1 Chemical formulae of the ditopic macrocycles H_6L^1 and H_8L^2 (with Schiff-base head units highlighted in magenta). H_6L^1 has been reported previously.[49]

have been functionalized with organic chromophore units in order to sensitize Ln-based luminescence.[43–48] Bimetallic lanthanoid complexes based on (Thia-)calix[4]arenes are rather rare.

Recently we have reported a ditopic macrocycle H_6L^1 comprising two calixarene and two bis(iminomethyl)phenyl head units (Fig. 1). This ligand supports dinuclear mixed-ligand complexes of the composition $[Ln_2L^1(H_2O)_2]$ (Ln = La^{3+}, Eu^{3+}, Tb^{3+}, Yb^{3+})[49] comprising two seven-coordinated Ln^{3+} ions.[50,51] The Schiff-base units act as antennae thus enabling sensitization of Eu^{III} and Tb^{III} luminescence emission under irradiation with UV light in the solid state (λ_{ex} = 370 nm).

We have now investigated the synthesis of related Ln^{3+} complexes derived from the macrocycle H_8L^2 in which the bis(iminomethyl)phenyl linkers have been replaced by bis(iminomethyl)biphenyl units, which changes the rigidity and size of the system. We found that H_8L^2 is an effective ditopic ligand stabilizing dinuclear macrocyclic lanthanide complexes of composition $[Ln_2(H_2L^2)(H_2O)_2]$ (Ln = La^{3+} (**1**), Eu^{3+} (**2**), Tb^{3+} (**3**), and Yb^{3+} (**4**)). Herein, their structures and photophysical properties are reported and compared with the previously published $[Ln_2(L^1)(H_2O)_2]$ complexes.[49] We also briefly examined the possibility of synthesizing the heterodinuclear Eu^{III}/Tb^{III} complex (**5**) in order to study a potential energy transfer process between the two Ln ions.

Results and discussion

Synthesis and characterization of H_8L^2

The macrocyclic ligand H_8L^2 was prepared by a [2+2] Schiff-base condensation reaction according to literature procedures as illustrated in Scheme 1.[52,53] The two precursors 25,27-bis-(aminoethoxy)-26,28-dihydroxy-calix[4]arene and dihydroxy-4,4′-biphenyldicarbaldehyde reacted readily in a 1 : 1 stoichiometric ratio in a mixed CH_2Cl_2/EtOH solution at room temperature and provided the macrocycle as a yellow product. The low solubility of H_8L^2 drives the reaction to near completion with an almost quantitative yield (98%).

The new ligand gave satisfactory elemental analysis and was further identified by ESI mass spectrometry, FTIR, UV-vis, ^{1}H and ^{13}C NMR spectroscopy, and by X-ray crystallography. Fig. S2 (ESI†) displays the ^{1}H-NMR spectrum for H_8L^2 in CD_2Cl_2 along with the assignments of the NMR signals. The two intense peaks at 1.15 and 1.24 ppm are attributed to the *tert*-butyl groups. The calix[4]arene methylene groups give rise to two AB spin systems centered at 3.41 ppm and 4.35 ppm. This spectral feature is consistent with the presence of a cone conformation for the calix[4]arene[54] as also observed for H_6L^1.[49] The CH_2 groups of the ethylene linkers give rise to two triplets at 4.09 and 4.27 ppm, respectively. The four signals at 6.96, 7.05, 7.07 and 7.20 ppm are due to the aromatic protons. Two broad signals are seen for phenolic hydroxyl groups at 8.06 and 13.09 ppm indicating that they are involved in hydrogen bonding interactions. The four imine protons give rise to one singlet at 8.74 ppm. The ^{13}C NMR spectrum for H_8L^2 in CD_2Cl_2 reveals only 22 signals for the 124 C atoms.

Synthesis and characterization of lanthanide complexes (1–4)

The reaction of H_8L^2 with $La(NO_3)_3{\cdot}6H_2O$ and triethylamine as a base in a 1 : 2 : 8 molar ratio in MeOH/CH_2Cl_2 results in the formation of a yellow precipitate of the composition $[La_2(H_2L^2)(H_2O)_2]$ (**1**, where $(H_2L^2)^{6-}$ represents the sixfold deprotonated form of the ligand) in good yield (65%) (Scheme 2). The analogously synthesized Eu^{3+} (**2**), Tb^{3+} (**3**), and Yb^{3+} (**4**) complexes were obtained in a similar good yield.

The complexes are air stable solids, which are moderately soluble in cyclohexane and insoluble in other common organic

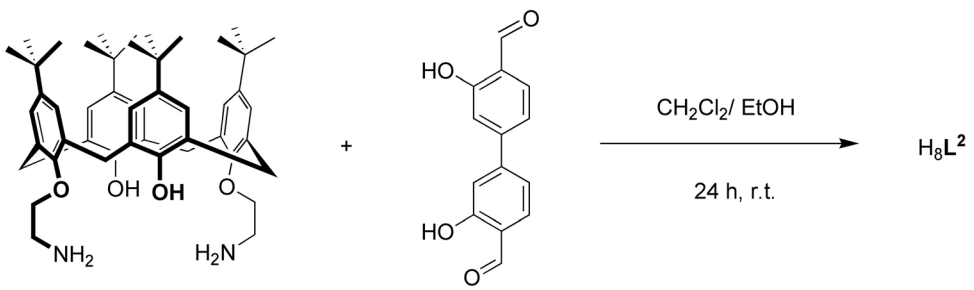

Scheme 1 Synthesis of the ligand H_8L^2.

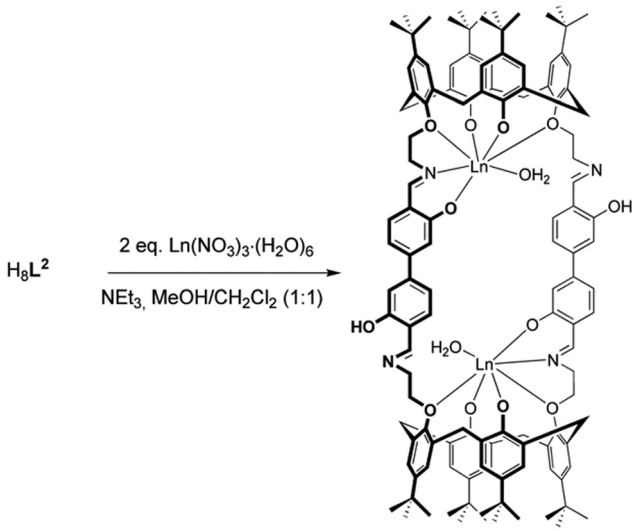

Scheme 2 Synthesis of the complexes $[Ln_2(H_2\mathbf{L}^2)(H_2O)_2]$ (Ln = La (**1**), Eu (**2**), Tb (**3**), Yb (**4**).

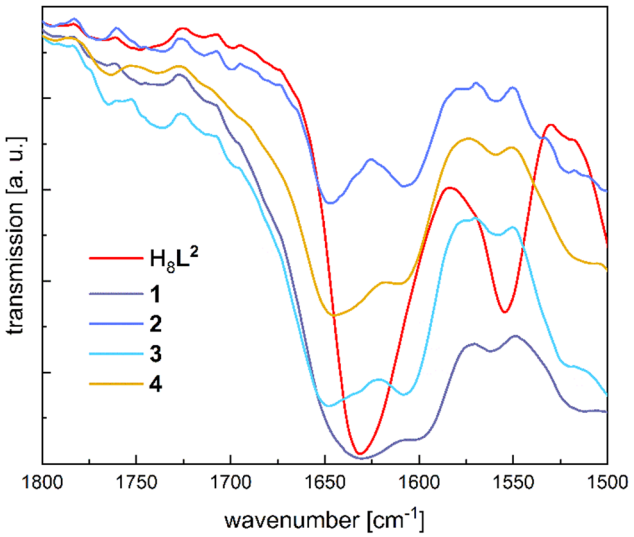

Fig. 2 Section of the ATR-FTIR Spectra of $H_8\mathbf{L}^2$ and the complexes **1–4** in the 1800–1500 cm^{-1} region.

Table 1 Selected FTIR and diffuse reflectance UV/Vis data for the ligand $H_8\mathbf{L}^2$ and the lanthanide complexes **1–4** and their assignments

Compound	$\tilde{\nu}^a$/cm^{-1}	$\lambda_{max}{}^b$/nm
$H_8\mathbf{L}^2$	3425 $\nu(H_2O)/\nu$(R–OH)	294 nm (π–π* calixarene)
	1631 (ν(C═N))	306 nm (sh, π–π* calixarene)
	1362, 1484 (δ(–N–CH_2–))	340 nm (π–π*, PhCH═NR)
		428 nm (sh, n–π*, PhCH═NR)
1	3424 $\nu(H_2O)/\nu$(R–OH)	294 nm (sh, π–π* calixarene)
	1631, 1602 (C═N)	306 nm (π–π* calixarene)
	1385, 1481 (δ(–N–CH_2–))	340 nm (sh, π–π*, PhCH═NR)
		406 nm (sh, n–π*, PhCH═NR)
2	3440 $\nu(H_2O)/\nu$(R–OH)	292 nm (sh, π–π* calixarene)
	1653, 1607 (C═N)	308 nm (π–π* calixarene)
	1385, 1477 (δ(–N–CH_2–))	342 nm (sh, π–π*, PhCH═NR)
		406 nm (sh, n–π*, PhCH═NR)
3	3417 $\nu(H_2O)/\nu$(R–OH)	294 nm (sh, π–π* calixarene)
	1647, 1608 (C═N)	308 nm (π–π* calixarene)
	1385, 1481 (δ(–N–CH_2–))	342 nm (sh, π–π*, PhCH═NR)
		406 nm (sh, n–π*, PhCH═NR)
4	3414 $\nu(H_2O)/\nu$(R-OH)	294 nm (sh, π–π* calixarene)
	1647, 1608 (C═N)	308 nm (π–π* calixarene)
	1385, 1482 (δ(–N–CH_2–))	342 nm (sh, π–π*, PhCH═NR)
		406 nm (sh, n–π*, PhCH═NR)

[a] ATR-mode. [b] Solid state UV/Vis diluted in $BaSO_4$, sh = shoulder.

solvents. All new compounds were further characterized by ESI mass spectrometry, ATR-FTIR, UV/Vis spectroscopy, and luminescence spectroscopy. The Yb^{3+} complex **4** was additionally identified by X-ray crystallography. Selected analytical data are listed in Table 1.

FTIR spectra of **1–4** (powder spectra) were recorded in the ATR mode. Fig. 2 shows a comparison of the ATR-FTIR spectra of $H_8\mathbf{L}^2$ and the complexes **1–4** in the 1800–1500 cm^{-1} range. The spectrum of $H_8\mathbf{L}^2$ reveals one intense absorption band at 1631 cm^{-1}, typical for the imine (ν(C═N)) stretching vibration.[55] In contrast to the free ligand, all complexes display two ν(C═N) absorption bands between 1650 and 1600 cm^{-1}, indicative of the presence of two kinds of imine groups (*i.e.* coordinating and free imine groups). Likewise, one of the deformation vibrations (wagging or twisting)[56] of the CH_2 group next to the imine observed for $H_8\mathbf{L}^2$ at 1362 cm^{-1} are shifted to higher frequencies in the complexes (1385 cm^{-1}), indicating the coordination of Ln^{3+} ions to the corresponding imine.[55] The broad feature at 3400 cm^{-1} does not disappear after coordination of lanthanide ions (Fig. S10–S14, ESI†). The vibrations are tentatively assigned to the O–H stretching vibrations of the Ln^{3+} bound water molecules.

Given the low solubility of the complexes **1–4**, all UV/Vis spectra were recorded in diffuse reflectance mode. The reflectance data were converted to absorption utilizing the Kubelka–Munk function.[57] The spectrum of the free ligand $H_8\mathbf{L}^2$ (Fig. 3) shows strong absorption bands at 294 nm and 340 nm. The former maximum exhibits a shoulder at ~306 nm. There is also another shoulder around 428 nm with lower intensity. The two low-energy absorptions are most likely associated with π–π* or n–π* transitions centered on the hydroxy-iminomethyl-functionalized biphenyl linkers. In agreement to the literature, π–π* transitions centered on the phenol ether and phenol groups of the calix[4]arene backbone absorb at the peak at 294 nm[58] and the parent biphenyl system absorbs at 306 nm.[59]

The diffuse reflectance UV/Vis spectra of the Ln complexes **1–4** differ only slightly from that of the free ligand. All complexes exhibit strong asymmetric absorption maxima at 306 nm with a shoulder at 294 nm. Absorption maxima at 340 nm and 406 nm also appear as shoulders in the spectrum. A slight hypsochromic shift of the n–π* transition centered on the hydroxy-iminomethyl-functionalized biphenyl linkers can be observed relative to the free ligand $H_8\mathbf{L}^2$. This shift can be traced to the coordination of the lanthanide ions. A similar behavior was reported for related Ln^{3+} complexes of other Schiff-base/calix[4]arene complexes.[60]

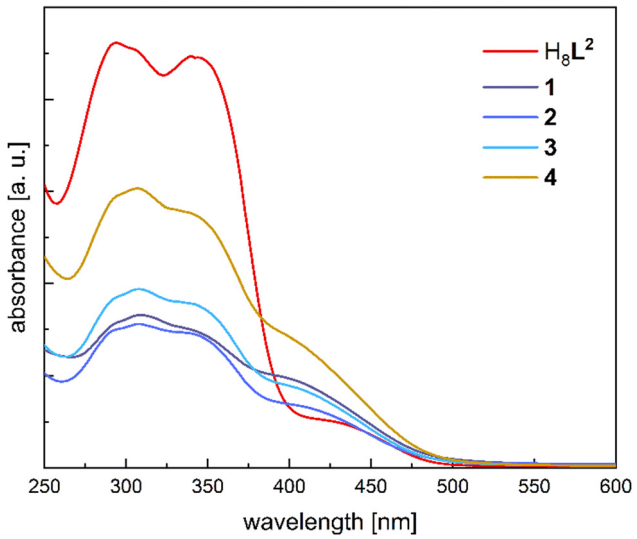

Fig. 3 Diffuse reflectance UV/Vis Spectra of $H_8\mathbf{L}^2$ and the complexes **1–4** measured as neat solids inside an integration sphere.

A comparison of the electronic absorption spectra of $H_8\mathbf{L}^2$ with those of $H_6\mathbf{L}^1$ shows many similarities. Differences can be seen for the π−π* transitions of the calixarene units as well as the n–π* transition of the iminophenol units of $H_8\mathbf{L}^2$, which are shifted bathochromically (by 18 nm) relative to those of $H_6\mathbf{L}^1$.[49] The π−π* transitions of the bis(iminomethyl)biphenyl linkers in $H_8\mathbf{L}^2$, on the other hand, are not shifted relative to those of the iminophenol units in $H_6\mathbf{L}^1$ which is not surprising in view of the twisting of the biphenyl linkers (that does not lead to a more extended π-system in $H_8\mathbf{L}^2$). The UV/Vis spectral data for a corresponding set of two complexes $[Ln_2(\mathbf{L}^1)(MeOH)_2]$ and $[Ln_2(H_2\mathbf{L}^2)(H_2O)_2]$ are also similar, as far as the calix[4]arene chromophores are concerned.[49] There are, however, significant differences in the positions of the n–π* transitions of the imino phenolate units in the two complexes. These differences may be due to the different types of second-sphere hydrogen-bonding interactions. The Ln bound solvate molecules in the $[Ln_2(H_2\mathbf{L}^2)(H_2O)_2]$ complexes, for example, are involved in hydrogen bonding interactions with the calix[4]arene O atoms, whereas they are involved in direct H-bonds with the non-coordinating imino-phenolate N atoms in the $[Ln_2(\mathbf{L}^1)(H_2O)_2]$ complexes (see below), which will exert an effect on the energy of the orbitals involved in the electronic transitions.

Crystallographic characterization

Description of the crystal structure of $H_8\mathbf{L}^2\cdot 4CH_2Cl_2$. Single crystals of $H_8\mathbf{L}^2\cdot 4CH_2Cl_2$ picked from the reaction mixture were subjected to X-ray crystallographic analysis. $H_8\mathbf{L}^2\cdot 4CH_2Cl_2$ crystallizes triclinic, space group $P\bar{1}$. The crystal structure is composed of discrete $H_8\mathbf{L}^2$ molecules (shown in Fig. 4) and co-crystallized CH_2Cl_2 solvate molecules. Each calix[4]arene group accommodates one CH_2Cl_2 molecule, which interacts with the electron-rich aryl rings *via* CH···π interactions (Fig. 5). The other CH_2Cl_2 molecules are enclathrated in the voids generated by the specific packing of the $H_8\mathbf{L}^2$ molecules. The individual $H_8\mathbf{L}^2$ molecules exhibit crystallographically imposed inversion symmetry. The molecules exhibit an overall "S-shape" structure, with the calix[4]arenes each bent away from an imaginary axis passing along the direction of the biphenyl moieties.

The calix[4]arene units adopt the cone conformation in agreement with the ^{1}H NMR data. The aryl rings of the biphenyl moieties are twisted by 37.16° which is a typical value for the biphenyl system.[61] This twisting prevents intramolecular π–π stacking interactions between the two biphenyl linkers, despite the fact that they are held in close proximity by the calix[4]arene groups (closest intramolecular C···C distance between biphenyl groups at 3.557 Å (C31···C33′)). All Schiff-base groups are nearly planar, stabilized by intramolecular OH···N hydrogen bonding interactions typical for *O*-hydroxyaryl Schiff bases. Intramolecular OH···O hydrogen bonding interactions are also present between the phenol and phenolether units of the calix[4]arene (*e.g.* O2···O5′ = 2.710 Å).

Self-assembly of the "S-shape" molecules within the crystal structure shows a bilayer arrangement with alternating calix[4]-arene and biphenyl segments. The thicknesses of the two layers were found to have similar values of approx. 5 Å and 8 Å, respectively (Fig. 6). Hierarchical self-assembly of calix[4]arene molecules (resembling that of mineral clays) has precedence in the literature.[62,63]

Description of the crystal structure of $[Yb_2(H_2\mathbf{L}^2)(H_2O)_2]\cdot 2H_2O\cdot 1.5MeCN$ ($4\cdot 2H_2O\cdot 1.5MeCN$)

Single crystals of $[Yb_2(H_2\mathbf{L}^2)(H_2O)_2]\cdot 2H_2O\cdot 1.5MeCN$ ($4\cdot 2H_2O\cdot 1.5MeCN$) obtained from a mixed solvent system (MeOH/MeCN)

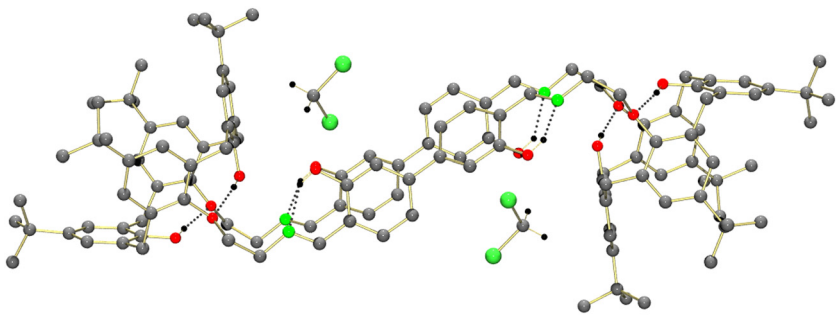

Fig. 4 Ball and stick representation of the molecular structure of compound $H_8\mathbf{L}^2$ as determined by single-crystal X-ray diffraction. H atoms except those involved in hydrogen bonding interactions and CH_2Cl_2 molecules situated in the cavities of the calix[4]arenes have been omitted for clarity.

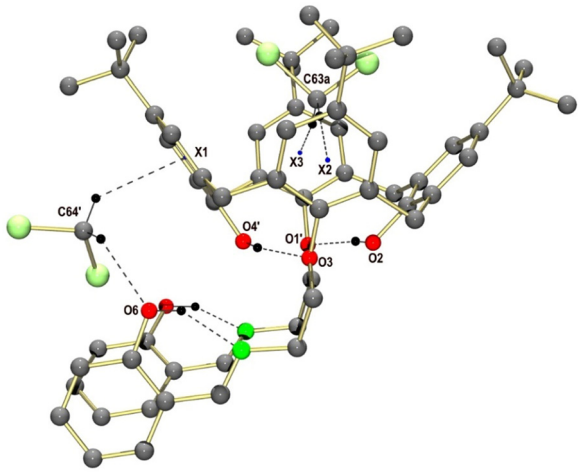

Fig. 5 Representation of the intermolecular CH···π interactions between the CH_2Cl_2 solvate molecules and the calix[4]arene units of $H_8\mathbf{L}^2$. Parts of the ligands have been omitted for clarity. Only one orientation of the disordered CH_2Cl_2 molecule is displayed. Symmetry code used to generate equivalent atoms: $1-x$, $1-y$, $1-z$ (′). Selected distances/Å: C63a···X2 (center of aryl ring) 3.422, C63a···X3 3.671, C64′···X1 3.375, C64′···O6 3.249.

are monoclinic, space group $P2_1/c$. Although the quality of the X-ray data is quite low, it can confirm the atom connectivity. The crystal structure is composed of discrete, dinuclear $[Yb_2(H_2\mathbf{L}^2)(H_2O)_2]$ complexes and co-crystallized H_2O and CH_3CN solvate molecules. Fig. 7 shows the structure of the dinuclear ytterbium complex. The $[Yb_2(H_2\mathbf{L}^2)(H_2O)_2]$ complexes exhibit crystallographically imposed inversion symmetry. Each Yb ion is seven-coordinated by the four calix[4]arene O atoms, the imine N and O atoms of one of the two Schiff base linkers, and one H_2O molecule. The coordination geometry is intermediate between distorted mono-capped trigonal prismatic (shape[64,65] symmetry factor: 1.669) and mono-capped octahedral (symmetry factor: 0.879), which are common coordination geometries for seven coordinate lanthanide complexes.[50,51]

The Yb–O bond lengths in **4** span a rather broad range from 2.08 to 2.50 Å. The Yb–O bond lengths appear to depend on the type of O donor. They increase in the following order: $Yb–O^{phenolate} < Yb–O^{iminophenolate} < Yb–O^{H_2O} < Yb–O^{arylether}$ (O1, O3 phenolether). This ranking of Yb–O bonds reflects the different donor abilities of the four types of O donors, with the two extremes represented by the hard, charged phenolate (O2, O4) and the neutral phenolether functions (O1, O3) of the calixarenes. The weaker donor ability of the iminophenolate functions can be traced to electron withdrawing effects of the imine functions, which reduce the electron density of the phenolato donors. The stronger electron delocalization in the iminophenolate group is also manifested by a shorter $Ar^C–O$ bond length (1.32 Å for the iminophenolate group *vs.* 1.35 Å for the phenolate of the calixarene). The H_2O donor is comparable in donor ability to the phenol ether O atoms. The $Yb–N^{imine}$ bonds are only slightly larger than the $Yb–O^{H_2O}$ bonds (2.406 *vs.* 2.421 Å). The intramolecular Yb···Yb distance in **4** amounts to 15.9 Å, and is thus much longer than the shortest intermolecular Yb···Yb distance of 9.1 Å.

The mutual arrangement of the two biphenyl linkers in the Yb complex is quite different from that observed for the free ligand, although the overall ''S-shape'' structure is maintained. Thus, unlike in $H_8\mathbf{L}^2$, the two non-coordinating Schiff-base units in **4** are co-planar towards each other and are more shifted relative to each other than in the free ligand (distance of the center of the biphenyl moiety = 8.5 Å (**4**) *versus* 4.3 Å ($H_8\mathbf{L}^2$)). Nevertheless, the biphenyl moieties are still twisted as in the free ligand. The Yb complexes pack in a similar fashion as the $H_8\mathbf{L}^2$ ligand, with the biphenyl and Yb-calix[4]arene entities arranged in 2D sheets (Fig. S25, ESI†).

We have also been able to grow single-crystals of the La complex **1**. Although the quality of the data set is not as good as desirable for publications, it can prove the atom connectivity. According to this data set, the La complex **1** is isostructural with the Yb complex **4**. Therefore, the La atom in **1** exhibits the same coordination environment and coordination number as the Yb atom in complex **4**. Thus, we believe that all the Ln complexes presented in this series form an isostructural set of complexes. This behavior may be related to the rigid constraints imposed by the macrocyclic calix[4]arene ligand. We have observed a similar behavior for a set of bimetallic Ln complexes supported by a calix[4]arene ligand bearing a pendant picolyl-imine arm.[66] For other complexes with less constrained ligands, it is not uncommon that the coordination

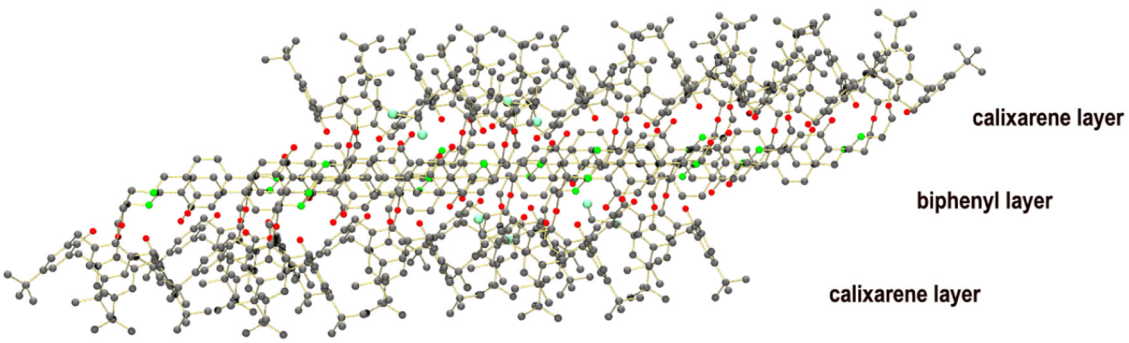

Fig. 6 Self-assembled structure of the ligand $H_8\mathbf{L}^2$, depicting segregation into alternating layers of biphenyl and calix[4]arene moieties (view is normal to (010)).

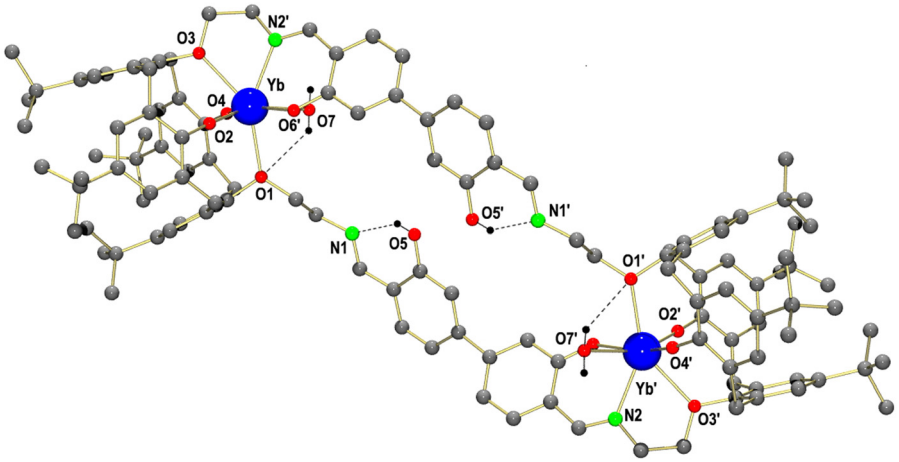

Fig. 7 Single-crystal X-ray diffraction structure of $[Yb_2(H_2\mathbf{L}^2)(H_2O)_2]\cdot 2H_2O\cdot 1.5MeCN$ (**4**·$2H_2O$·1.5MeCN) (ball-and-stick representation). H_2O and MeCN solvate molecules as well as H atoms (except those involved in H bonding interactions) are omitted for clarity. Dashed lines refer to intramolecular hydrogen bonding interactions (O7···O1 = 3.060 Å, O5···N1 = 2.551 Å, O5···O5′ = 3.153 Å). Symmetry code used to generate equivalent atoms $1-x, -y, -z$ (′).

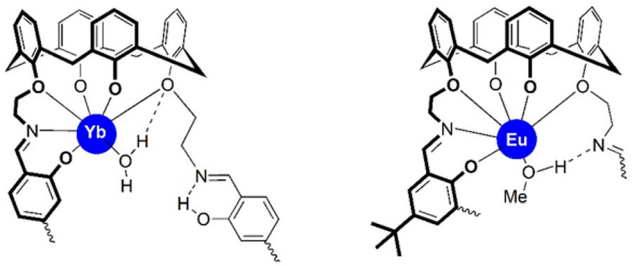

Fig. 8 Comparison of the immediate coordination environments in $[Yb_2(H_2\mathbf{L}^2)(H_2O)_2]$ (**4**) (left) and in $[Eu_2(\mathbf{L}^1)(MeOH)_2]$ (right). Parts of the structures were omitted for clarity.

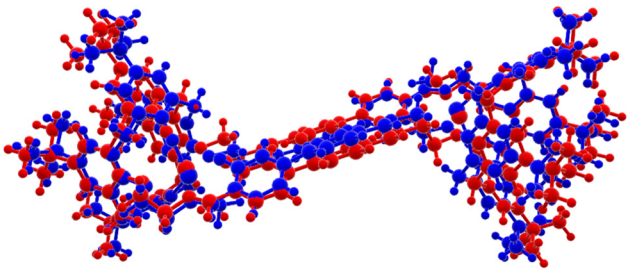

Fig. 9 Structural differences between XRD derived and DFT optimized structure. Blue: XRD derived structure of **4**, red: DFT optimized structure of **1**.

number decreases by one unit when the Ln series is traversed from the left to the right.[67]

It should be mentioned, that the coordination mode of the ligand $H_8\mathbf{L}^2$ in **4** is very similar to that of the ligand $H_2\mathbf{L}^1$ in the europium complex $[Eu_2(\mathbf{L}^1)(MeOH)_2]$ (Fig. 8).[49] Thus, each macrocycle utilizes all four calix[4]arene O atoms and the N and O donors of just one Schiff base unit in the coordination of a Ln^{3+} ion. The other Schiff base moiety remains free as in **4** or in the $[Ln_2(H_2L_1)(MeOH)_2]$ complexes. The ligands are thus bis-hexadentate ligands comprising of two O_5N binding pockets. Thus, as observed before,[49] one additional co-ligand is coordinated to the lanthanide ions to saturate its coordination demands. The similarity in the coordination environments is also illustrated by the shape factors, which provide a measure for the deviation from the ideal coordination environments. Thus, irrespective of the type of Schiff base linkers only seven-coordinated Ln complexes can be accommodated, most likely due to the steric demand of the macrocyclic structures.

DFT calculations

So far, we have not been able to grow single crystals of the other lanthanide complexes suitable for structure determination. Therefore, density functional theory (DFT) calculations were carried out for the complex $[La_2(H_2\mathbf{L}^2)(H_2O)_2]$ (**1**) (r^2SCAN, def2-mTZVPP, 3c (D4+gcp) level of computation). The calculated and experimental structures of **1** and **4** compare reasonably well with each other (Fig. 9). The main difference between the calculated and experimental structures is, as expected, an increase of the average M–O and M–N distances of 0.22 Å (Table S2, ESI†) in the calculation of **1** compared to the experimental structure of **4**. This is in agreement with the larger atomic radius of the lanthanum ion in **1** compared to the ytterbium ion in **4**.[68] Compensating for the difference in the ion radius results in an average distance difference of 0.07 Å for the M–O and M–N bonds. The average M–O bond lengths are *ca.* 0.078 Å different (absolute differences) and the M–N bond is on average 0.01 Å longer in the calculated structure of **1** (Table S2, ESI†). The bond angles around the lanthanum atom in the optimized structure of **1** deviate from the experimental structure of **4** by a maximum of 19.9° with an average deviation of 6.5° (*e.g.* O2–La–O6 137.6 *vs.* 157.6(5)°) (Tables S3 and S4, ESI†). Based on these calculations, we conclude that all the Ln complexes supported by $H_8\mathbf{L}^2$ adopt the same structures.

We also optimized a MeOH solvated complex using the same methodology. Again, the calculated structure for this compound agreed well with the experimental structure for **4**. It can be

concluded that MeOH ligands can be accommodated in the coordination sphere of the Yb complexes as well. The difference of the reaction free energy for complexation reaction: (2 La^{3+} + $(H_2\mathbf{L}^2)^{6-}$ + 2 L′ → $[La_2(H_2\mathbf{L}^2)(L')_2]$) between water and methanol was calculated to be $\Delta\Delta G$ = 4.7 kJ mol^{-1}, indicating that water binds only slightly stronger than methanol. In other words, the co-ligand L′ in the $[La_2(H_2\mathbf{L}^2)(L')_2]$ complex is exchangeable from a thermodynamic perspective. This behavior has also been observed for dinuclear lanthanide complexes supported by $H_2\mathbf{L}^1$.[49]

Spectroscopic and photophysical properties

$H_8\mathbf{L}^2$ and complexes **1–4** were characterized by photoluminescence spectroscopy to probe a potential sensitization of the emission of the coordinated lanthanide ions (antenna effect). Photoluminescence spectra were recorded for the neat solids at room temperature. Fig. 10 displays an overlay of the photoluminescence spectra for the free ligand and the Eu (**2**) and Tb (**3**) complexes. The spectrum for $H_8\mathbf{L}^2$ displays a very broad emission band at 556 nm under excitation with 370 nm UV-radiation, which can be attributed to emission from a π–π* state located on the bis(iminomethyl)biphenyl system. The spectrum of the Eu complex also displays a similar broad emission band with a maximum at 560 nm, however, the emission intensity is reduced, relative to that of the free ligand. The spectrum of the Eu complex **2** displays also several line-like emission bands at 579 nm, 591 nm, 614 nm, 649 nm, and 685–701 nm attributed to the characteristic $^5D_0 \rightarrow {}^7F_J$ transitions (J = 0–4) from the excited $^5D_0$ state of the Eu^{3+} ion.[69] The appearance of the emission maximum at 579 nm attributed to the $^5D_0 \rightarrow {}^7F_0$ transition is in good agreement with the low local C_1 symmetry of the coordination environment about the Eu^{3+} ions.[69] However, a potential splitting of the $^5D_0 \rightarrow {}^7F_1$ and the $^5D_0 \rightarrow {}^7F_2$ transitions due to crystal field effects, which is typically observed for seven-coordinated Eu Schiff-base complexes,[70] is not observed under our conditions.

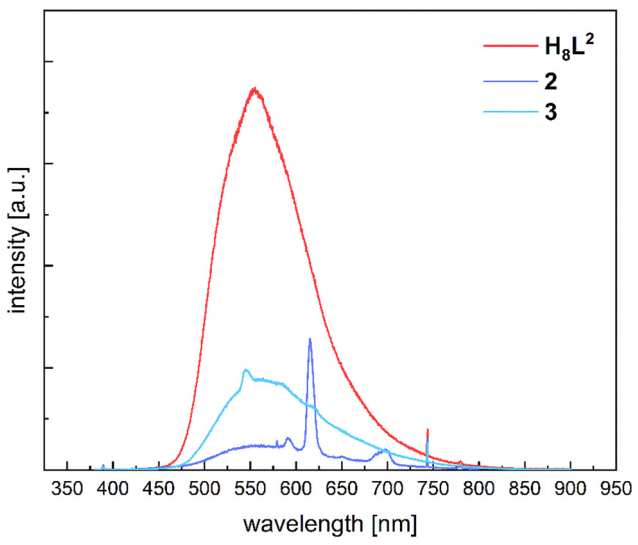

Fig. 10 Photoluminescence spectra of $H_8\mathbf{L}^2$, $[Eu_2(H_2\mathbf{L}^2)(H_2O)_2]$ (**2**) and $[Tb_2(H_2\mathbf{L}^2)(H_2O)_2]$ (**3**) at 295 K (neat solids). The excitation wavelength is 370 nm. The Ln transitions start from the $^5D_0$ state of the Eu^{3+} and the $^5D_4$ state of the Tb^{3+} ion.

The photoluminescence spectrum for the Tb complex also shows a broad emission band with a maximum at 560 nm. The reduction of the intensity relative to the free ligand is less pronounced than in the Eu complex. The weak, line like emission maxima centered at 545 nm, 585 nm, and 618 nm, can be attributed to the $^5D_4 \rightarrow {}^7F_J$ (J = 5, 4, 3) transitions from the excited $^5D_4$ state of the Tb^{3+} ion. The $^5D_4 \rightarrow {}^7F_6$ transition (expected at 480 nm) is not observed.

The excitation spectra of the Eu and Tb complexes monitored at 620 nm and 540 nm, respectively, show broad absorption bands in the 300 to 450 nm range (Fig. S26, ESI†). These are attributed to the transitions into the $^1(\pi–\pi^*)$ state of the bis(iminomethyl)phenolato ligand, clearly showing that they can function as an antenna for sensitizing the Eu^{3+} and Tb^{3+} ions. This is also in line with previous work, where we determined triplet state energies of several Schiff-base substituents appended to calix[4]arene-ligands. All were found to lie well above the $^5D_4$ and $^5D_0$ resonance levels of the Tb^{3+} and Eu^{3+} ions (~20.500 cm^{-1} and ~17.500 cm^{-1}, respectively).[71] The triplet state energy in the parent 2-(methylphenol)imino-ethoxy substituent (which is also part of the present ligand system), for example, is found at 21 882 cm^{-1}.[49] The fact that the emission of the ligand is also observed can be traced to the fact that one of the Schiff-base units in the linking biphenyl groups is not coordinated to the lanthanide ions.

Photophysical properties of a heterodinuclear Eu/Tb complex

It was of interest to synthesize a heterodinuclear $[TbEu(H_2\mathbf{L}^2)(H_2O)_2]$ (**5**) complex and to investigate its photoluminescence properties, in view of literature reports that such complexes give rise to energy transfer between the Tb^{3+} and Eu^{3+} ions.[14] Thus, in an orienting experiment the ligand $H_8\mathbf{L}^2$ was reacted with a 1 : 1 mixture of $Eu(NO_3)_3{\cdot}6H_2O$ and $Tb(NO_3)_3{\cdot}6H_2O$ to afford a material containing the heterodinuclear complex $[EuTb(H_2\mathbf{L}^2)(H_2O)_2]$ (**5**). The presence and thus successful synthesis of **5** was validated by ESI-MS spectrometry (Fig. S8, ESI†). Fig. 11 displays the photoluminescence spectrum of this material. Only the characteristic emission maxima for the Eu(III) complexes luminescence are discernible. The characteristic emission band for the Tb(III) centers, as for instance the maximum centered at 545 nm, is no longer present (or greatly reduced in intensity). Moreover, the luminescence lifetime for **5** is significantly reduced (178 μs in **2** to 57 μs in **5**) than observed for compound **2** under the same experimental conditions (Table S7, ESI†). The obtained luminescence excitation spectra show a decrease in energy from 445 nm in **2** (and a 1 : 1 mixture of **2** and **3**) to 465 nm in **5** (Table S6, ESI†). These results may be traced to intermolecular energy transfer processes between the Tb(III) and Eu(III) centers. Intermolecular energy transfer processes have been observed in other heterometallic Tb/Eu complexes.[16] For efficient intermetallic communication such as an energy transfer distances between interacting Ln ions must be reduced below 3.5–4 Å for an orbital overlap (Dexter energy transfer) or below 10 Å for efficient dipolar

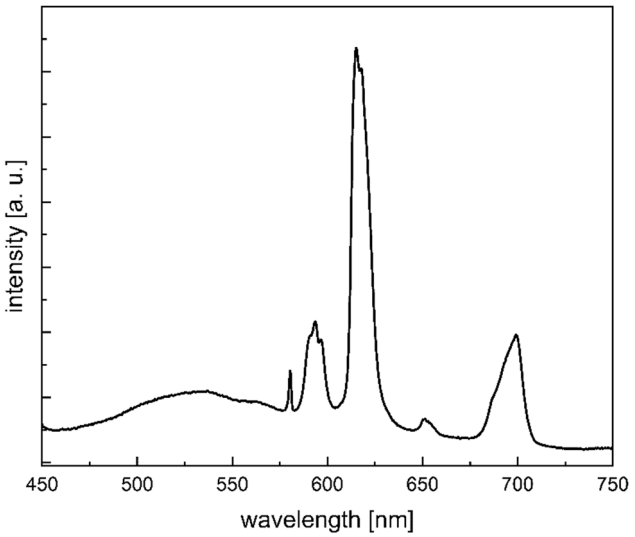

Fig. 11 Photoluminescence spectra of [EuTb(H_2**L**^{2})(H_2O)$_2$] (**5**) at 295 K (neat solids). The excitation wavelength is 370 nm.

through-space interactions (Förster resonance energy transfer).[16] Based on the results of X-ray diffraction and DFT calculations we can safely assume that intramolecular distances between Eu and Tb centers are in the range of 16 Å and intermolecular distances between metal centers are in the range of 9 Å. Based on these distances an intermolecular energy transfer is presumably more likely than an intramolecular one.

Conclusion

A new ditopic calix[4]arene-Schiff base ligand, comprising two calix[4]arene head units linked by two 3,3′-dihydroxy-4,4′-biphenyldicarbimin units, has been synthesized and its coordination chemistry towards selected lanthanide ions (La^{3+}, Eu^{3+}, Tb^{3+}, Yb^{3+}) investigated in solution and solid state. H_8**L**^{2} was found to act as a bis-hexadentate ligands comprising two O_5N binding pockets. Since it cannot saturate the coordination demands of the Ln^{3+} ions, one additional co-ligand is coordinated to the lanthanide ions to produce mixed-ligand complexes of composition [Ln_2(H_2**L**^{2})(H_2O)$_2$]. The Yb^{3+} ions are seven-coordinated in a distorted monocapped trigonal prismatic coordination environment (NO_6 donor set). DFT calculations for the La complex **1** (at the r^{2}SCAN-3c level of computation) implies an isostructural series of compounds. The electronic absorption spectra of the [Ln_2(H_2**L**^{2})(H_2O)$_2$] complexes reveal strong absorption maxima in the 250–440 nm range ($\varepsilon > 10^4$ M^{-1} cm^{-1}) attributed to ligand-based π–π* and n–π* transitions. The enlarged bis(iminomethyl)-biphenyl linkers in comparison to H_6**L**^{1} were found to sensitize Eu^{III} and Tb^{III} emission (λ_{ex} = 370 nm and 405 nm) in the solid state at 295 K. A material containing statistically distributed Tb^{III} and Eu^{III} ions reveals upon 370 nm excitation only Eu^{3+} emission lines indicative of intermolecular energy transfer processes between the Ln^{3+} ions. The ability of the ligand H_8**L**^{2} to form heterodinuclear complexes may be further exploited in regard to understanding and applying tunable luminescent lanthanide complexes.

Experimental section

Materials and methods

All reagents and solvents were commercial grade and used without further purification. The precursors 25,27-di(aminoethoxy)-4-*tert*-butylcalix[4]arene and 3,3′-dihydroxy-[1,1′-biphenyl]-4,4′-dicarbaldehyde were synthesized according to the literature.[53,72,73] Melting points were determined with an Electrothermal IA9000 series instrument using open glass capillaries and are uncorrected. Mass spectra were obtained using the positive ion electrospray ionization modus (ESI) on a Bruker Daltronics ESQUIRE 3000 Plus ITMS or Impact II UHR Qq-TOF instrument. Infrared spectra (4500–600 cm^{-1}) were recorded at 2 cm^{-1} resolution on a Bruker-Vertex 80V FT-IR spectrometer using a diamond-ATR unit. The diffuse reflectance spectra were collected at room temperature on a Jasco V-670 UV-vis-NIR spectrophotometer with an ARN-914 absolute reflectance measurement unit, equipped with a photomultiplier and a PbS photoconductive cell. The complexes were mixed with $BaSO_4$ powder in a mortar to a content of 5% (by weight). The spectrum was collected in the 200–1600 nm range with a resolution of 2 nm. Diffuse reflectance UV-visible data were analyzed using a normalized absorbance, which is referred to as the KUBELKA–MUNK function,[57] $f(R_\infty)$, as shown in the following equation:

where R – diffuse reflectance of a sample is related to the absorption coefficient (K) and its scattering coefficient (S). Assuming the scattering coefficient being independent from the wavelengths, $f(R_\infty)$ is directly proportional to the absorption of the sample.

Synthesis and analysis of compounds

Calix[4]arene ligand H_8L^2. This compound was prepared by a modified literature procedure.[52] Thus, to a solution of 25,27-di(aminoethoxy)-4-*tert*-butylcalix[4]arene (200 mg, 272 μmol) in a mixed solvent system (EtOH/CH_2Cl_2 1 : 1, 30 mL) was added a solution of 3,3′-dihydroxy-[1,1′-biphenyl]-4,4′-dicarbaldehyde (66.0 mg, 272 μmol). The reaction mixture was stirred for 12 h at room temperature. The resulting yellow precipitate was filtrated, washed with ethanol, and dried in a vacuum. Yield: 251 mg (133 mmol, 49%). M.p.: > 300 °C (decomp). ATR-IR (diamond): ν/cm^{-1} = 3420, 2960, 2904, 2867, 1631, 1485, 1362, 1194, 1124, 1047, 872, 797. *m*/*z* (ESI+, MeCN): 1883.484 ([M + H$^+$], calc.: 1883.09). ^{1}H-NMR (400 MHz, CD_2Cl_2) δ = 13.09 (s, 4 H, *ipso* **H**O–Ar c[4]a); 8.74 (s, 4 H, N = C**H**), 8.06 (s, 4 H, *ortho* **H**O–Ar biphenyl), 7.20 (d, 4 H, ^3J = 8.06 Hz, *meta* **H**Ar biphenyl), 7.07 (d, ^3J = 1.3 Hz, 16 H, *meta* **H**Ar biphenyl), 7.05 (d, ^3J = 1.7 Hz, 4 H, *ortho* **H**Ar biphenyl), 6.96 (dd, ^3J = 8.0, 1.8 Hz, 4 H, *meta* **H**Ar (relative to imine) *ortho* **H**Ar (rel. hydroxy) biphenyl), 4.35 (d, ^2J = 12.8 Hz, 8 H, Ar–CH**H**$_{ax}$–Ar), 4.27 (t, ^3J = 6.1 Hz, 8 H, C═N–C**H**$_2$–CH$_2$–O), 4.09 (t, ^3J = 5.9 Hz, 8 H, C═N–CH$_2$–C**H**$_2$–O), 3.41 (d, ^2J = 12.9 Hz, 8 H, Ar–CH**H**$_{eq}$–Ar), 1.24

(s, 32 H, HO–Ar–C(CH_3)$_3$), 1.15 (s, 32 H, CH_2–O–Ar–C(CH_3)$_3$). ^{13}C NMR (75 MHz, CD_2Cl_2): δ = 166.92 (Ar–CH=N), 161.37 (C^{Ar}–OH(biphenyl)), 151.11 (C^{Ar}–Ar(biphenyl)), 150.39 (C^{Ar}–CH_2–Ar), 148.01 (C^{Ar}–CH_2–Ar), 143.75 (C^{Ar}–O–CH_2), 142.25 (C^{Ar}–OH(calixarene)), 133.04 (C^{Ar}–C–CH_3), 132.30 (C^{Ar}–H(biphenyl)), 127.45 ((C^{Ar}–C–CH_3)), 126.53 (C^{Ar}–H(calixarene)), 125.98 (C^{Ar}–H(calixarene)), 118.81 (C^{Ar}–CH=N), 117.70 (C^{Ar}–H(biphenyl)), 115.44 (C^{Ar}–H(biphenyl)), 76.01 (O–CH_2–CH_2–N), 59.23 (O–CH_2–CH_2–N), 34.49 (C(CH_3)$_3$), 34.08 (C(CH_3)$_3$), 32.65 (Ar–CH_2–Ar), 31.77 (C(CH_3)$_3$), 31.36 (C(CH_3)$_3$). Elemental analysis calc. (%) for $C_{124}H_{144}N_4O_{12}$ $2H_2O$ (1882, 53 + 36.04): C 77.63, H 7.78, N 2.92; found: C 77.69, H 7,73, N 2.72. UV/Vis (solid): λ_{max} = 362 nm, 434 nm, emission (λ_{ex} = 370 nm): λ_{max} = 556 nm.

Complex 1. To a solution of $H_8\mathbf{L}^2$ (25 mg, 13 μmol) and NEt_3 (16 μL, 115 μmol) in CH_2Cl_2 (5 mL) was added a solution $La(NO_3)_3{\cdot}6H_2O$ (12 mg, 26 μmol) in methanol (5 mL) at room temperature. The reaction mixture was stirred for 24 h. [$La_2(H_2\mathbf{L}^2)(H_2O)_2$] precipitated as a pale-yellow solid from the reaction mixture. The product was washed with ethanol and dried in high vacuum to constant weight to a yield of 19 mg (66%). M.p.: >300 °C (decomp), ESI-MS+ (*m*/*z*): 2360.144 ([M + H^+ + 2 CH_2Cl_2], calc.: 2360.78), ATR-IR (diamond): ν/cm^{-1} = 3420, 2955, 2904, 2869, 1631, 1602, 1482, 1385, 1193, 1123, 1044, 871, 793 cm^{-1}. Elemental analysis calc. (%) for $C_{124}H_{142}La_2N_4O_{14}{\cdot}3CH_2Cl_2$ $3H_2O$: C 61.04, H 6.21, N 2.24; found: C 61.93, H 6.153, N 2.36. UV/Vis: λ_{max} = 386 nm, emission (λ_{ex} = 370 nm): λ_{max} = 556 nm.

Complex 2. $H_8\mathbf{L}^2$ (50 mg, 26 μmol), NEt_3 (31 μL, 230 μmol), and $Eu(NO_3)_3{\cdot}6H_2O$ (33 mg, 53 μmol) were reacted in analogy to the procedure detailed above for the lanthanum complex to give 38 mg (65%) of [$Eu_2(H_2\mathbf{L}^2)(H_2O)_2$] as a yellow powder. M.p.: >300 °C (decomp.). ESI-MS (*m*/*z*): 2490.829 ([M–H^+ + 2 CH_2Cl_2 + 2 CH_3OH + CH_3CN], calc.: 2490.87). ATR-IR (Diamond): ν/cm^{-1} = 3420, 2954, 2927, 2678, 1647, 1653, 1636, 1607, 1472, 1385, 1313 cm^{-1}. ESI-MS+ (*m*/*z*): 2180.907 ([M + H^+], calc.: 2180.41). Elemental analysis calc. (%) for $C_{124}H_{142}Eu_2N_4O_{14}{\cdot}CH_2Cl_2{\cdot}5H_2O$: C 62.78, H 6.49, N 2.34; found: C 63.22, H 6.08, N 2.24. UV/Vis (diffuse reflectance): λ_{max} = 400 nm. Emission (λ_{ex} = 370 nm): λ_{max} = 579 nm, 591 nm, 614 nm, 649 nm, 685–701 nm.

Complex 3. $H_8\mathbf{L}^2$ (20 mg, 10 μmol), NEt_3 (12 μL 86 μmol), and $Tb(NO_3)_3{\cdot}6H_2O$ (10 mg, 21 μmol) were reacted in analogy to the procedure detailed above for the lanthanum complex to give 15 mg (65%) of [$Tb_2(H_2\mathbf{L}^2)(H_2O)_2$] as a yellow powder. M.p.: >300 °C (decomp.); ESI-MS+ (*m*/*z*): 2236.588 ([M + H^+ + CH_3CN–2CH_3OH], calc.: 2235.92). ATR-IR (Diamond): ν/cm^{-1} = 3420, 2926, 2954, 2854, 2678, 2492, 1647, 1608, 1480, 1385, 1303, 1202, 1123, 872, 825, 804 cm^{-1}. ESI-MS+ (*m*/*z*): 2194.894 ([M + H^+], calc.: 2194.33). Elemental analysis calc. (%) for $C_{124}H_{142}Tb_2N_4O_{14}{\cdot}3CH_2Cl_2{\cdot}3H_2O$: C 60.07, H 6.11, N 2.21; found: C 60.93, H 5.96, N 2.15. UV/Vis (diffuse reflectance): λ_{max} = 416 nm. Emission (λ_{ex} = 370 nm): λ_{max} = 545 nm, 585 nm, 618 nm.

Complex 4. $H_8\mathbf{L}^2$ (65 mg, 47.45 μmol), NEt_3 (29 μL, 393.83 μmol), and $Yb(NO_3)_3{\cdot}5H_2O$ (23 mg, 104.39 μmol) were reacted in analogy to the procedure detailed above for the Lanthanum complex to give 15 mg (14%) of [$Yb_2(H_2\mathbf{L}^2)(H_2O)_2$] as a yellow powder. M.p.: >300 °C (decomp.). ESI-MS+ (*m*/*z*): 2223.919 ([M + H^+], calc.: 2223.92). ATR-IR (diamond): ν/cm^{-1} = 3420, 2940, 2738, 2678, 2492, 1647, 1476, 1385, 1195, 1123, 1099, 1037, 825 cm^{-1}. elemental analysis calc. (%) for $C_{124}H_{142}$-$Yb_2N_4O_{14}{\cdot}6H_2O$: C 62.93, H 6.56, N 2.37; found: C 63.29, H 5.94, N 2.26. UV/Vis (diffuse reflectance): λ_{max} = 412 nm. Emission (λ_{ex} = 370 nm): λ_{max} = 556 nm.

Complex 5. $H_8\mathbf{L}^2$ (40 mg, 21.25 μmol) and NEt_3 (24 μL, 170 μmol) were dissolved in CH_2Cl_2, EtOH (1 : 1, 20 mL) and a solution of $Eu(NO_3)_3{\cdot}6H_2O$ (10 mg, 21 μmol) and $Tb(NO_3)_3{\cdot}6H_2O$ (9 mg, 21 μmol) in CH_2Cl_2, EtOH (1 : 1, 10 mL) was added. The solution was stirred at reflux for 48 hours to give 18 mg (40%) of [$EuTb(H_2\mathbf{L}^2)(H_2O)_2$] as yellow-orange powder. ESI-MS+ (*m*/*z*): 2187.92 ([M + H^+], calc.: 2187.90).

Crystallography

Suitable specimens of $H_8\mathbf{L}^2{\cdot}4CH_2Cl_2$, [$La_2(H_2\mathbf{L}^2)(H_2O)_2$]·$2H_2O$·(**1**·$2H_2O$) and [$Yb_2(H_2\mathbf{L}^2)(H_2O)_2$]·$2H_2O$·1.5MeCN (**4**·$2H_2O$·1.5MeCN) were selected and mounted on a cryoloop using perfluoropolyether oil. The data sets were collected at 180(2) K on a Stoe Stadivari X-ray diffractometer equipped with a GeniX 3D Cu-HF (Xenocx) microfocus X-ray source with a graded multilayer mirror (Cu-K$_\alpha$, λ = 1.54186 Å) and a hybrid pixel detector Pilatus3 300K (Dectris). Data processing was carried out with the Stoe X-Area software including a spherical absorption correction and scaling routine.[74] The structures were solved with SHELXT 2018/2[X2][75] using dual methods and refined by full-matrix least-squares techniques based on all data against F^2 using version 2018/3 SHELXL[75] and Olex2.[76] The coordinates of all non-hydrogen atoms were refined with anisotropic thermal parameters. Hydrogen atoms were included in idealized positions. Due to the low quality of the [$Yb_2(H_2\mathbf{L}^2)(H_2O)_2$]·$2H_2O$·1.5MeCN measurement, it was not possible to refine the position of the hydrogen atoms connected to the disordered solvent water molecule.

Crystallographic data for $H_8\mathbf{L}^2{\cdot}4CH_2Cl_2$

Crystallographic data for $H_8\mathbf{L}^2{\cdot}4CH_2Cl_2$. $C_{128}H_{152}Cl_8N_4O_{12}$, M_r = 2222.13 g mol^{-1}, triclinic, space group $P\bar{1}$, a = 12.1498(2) Å, b = 12.5940(3) Å, c = 20.1633(4) Å, α = 85.048(2)°, β = 84.743(2)°, γ = 83.090(2)°, V = 3041.13(11) Å^3, Z = 1, ρ_{calcd} = 1.213 g cm^{-3}, T = 180(2) K, μ(Cu-Kα) = 2.166 mm^{-1} (λ = 1.54186 Å), crystal size 0.249 × 0.215 × 0.186 mm^3, 52 723 reflections measured, 11 421 unique, 7253 with $I > 2\sigma(I)$. Final R_1 = 0.0614 ($I > 2\sigma(I)$), wR_2 = 0.1942 (all data), 729 parameters and 44 restraints, min./max. residual electron density = −0.54/0.26 e$^-$ Å^{-3}.

Crystallographic data for [$Yb_2(H_2\mathbf{L}^2)(H_2O)_2$]·$2H_2O$·1.5MeCN (**4**·$2H_2O$·1.5MeCN)

Crystallographic data for [$Yb_2(H_2\mathbf{L}^2)(H_2O)_2$]·$2H_2O$·1.5MeCN. $C_{127}H_{150.5}N_{5.5}O_{16}Yb_2$, M_r = 2356.10 g mol^{-1}, monoclinic, space group $P2_1/c$, a = 21.2650(12) Å, b = 13.1176(12) Å, c = 21.2994(11) Å, β = 114.929(4)°, V = 5894.6(7) Å^3, Z = 2, ρ_{calcd} = 1.327 g cm^{-3}, T = 180(2) K, μ(Cu-Kα) = 3.370 mm^{-1} (λ = 1.54186 Å), crystal size

0.270 × 0.213 × 0.140 mm^3, 25639 reflections measured, 6041 unique, 3089 with $I > 2\sigma(I)$. Final R_1 = 0.0885 ($I > 2\sigma(I)$), wR_2 = 0.2425 (all data), 676 parameters and 105 restraints, min./max. residual electron density = −0.40/1.59 e$^-$ Å^{-3}.

Crystallographic data for $[La_2(H_2L^2)(H_2O)_2]\cdot 2H_2O$ ($1\cdot 2H_2O$)

Crystallographic data for $[Yb_2(H_2L^2)(H_2O)_2]\cdot 2H_2O$. $C_{124}H_{146}La_2N_4O_{16}$, M_r = 2226.26 g mol^{-1}, monoclinic, space group $P2_1/c$, a = 23.283(2) Å, b = 13.1277(7) Å, c = 21.396(2) Å, β = 115.459(7)°, V = 5904.7(9) Å^3, Z = 2, ρ_{calcd} = 1.252 g cm^{-3}, T = 180(2) K, μ(Cu-K$_\alpha$) = 6.009 mm^{-1} (λ = 1.54186 Å), crystal size 0.057 × 0.029 × 0.024 mm^3, 35 888 reflections measured, 7414 unique, 2209 with $I > 2\sigma(I)$. Final R_1 = 0.1317 ($I > 2\sigma(I)$), wR_2 = 0.4352 (all data), 345 parameters and 12 restraints, min./max. residual electron density = −0.44/0.70 e$^-$ Å^{-3}.

The quality of the data set is not as good as desirable for publication. However, it can prove the atom connectivity. The cif file for **1** has been deposited in the CCDC.

Photophysical characterization

Photoluminescence spectra were recorded with an inverted confocal microscope (Olympus IX71) fiber coupled to a spectrometer (iHR320, synapse CCD, HORIBA JobinYvon). The light was focused and collected in a backscattering geometry by a 10× objective (Olympus LUCPlan FLN 10× NA 0.3). The excitation wavelength was 370 nm and 405 nm, respectively (equipped with a Becker & Hickl Diode Laser operating in CW mode).

The luminescence excitation spectra were determined using a Tecan microplate reader (Infinite 200 Pro, Tecan Trading AG) and UV transparent microplates. Observed emission wavelength was chosen according to the luminescence (λ_{em} = 520 nm for the ligand, λ_{em} = 540 nm for the terbium complex and λ_{em} = 620 nm for the europium complex). An integration time of 500 μs and number flashes of 100 were use for the measurement.

The luminescence lifetimes of the ligand and the complex were determined using a fluorescence lifetime imaging microscope (FLIM) and phosphorescence lifetime imaging microscope (PLIM) approach. The microscope is based on a DCS-120 FLIM system (Becker and Hickl) combined with an inverted confocal microscope (IX71, Olympus) equipped with 10× objective (Olympus MPlan 10× NA = 0.25) and a 435 long pass filter. For FLIM the excitation a 405 nm, 80 ps laserdiode (repetition rate 80 MHz) was applied. For the PLIM measurements of the complexes a burst of multiple laser pulses (LB) was applied for the excitation.

Density functional theory calculations

Pre- and postprocessing employed functionality from the PLAMS[77] and ASE[78] python packages. Plots have been produced using the matplotlib library,[79] and VMD[80] was used for structural representations. The full workflow including all scripts, plots, inputs, and outputs generated in this project are available on Zenodo.[81] General calculation settings are described below.

ORCA version 5.0.4[82,83] was used to perform restricted (spin-unpolarized) Kohn–Sham density-functional theory (DFT) calculations. The finest grid available in ORCA (input keyword "DEFGrid3") was used for all calculations. The SCF convergence criterion was set to "TightSCF" with the default convergence check mode and geometries were converged using the "TightOpt" keyword (see the ORCA manual for a list of all tolerance values set by these keywords). The *meta*-GGA r^{2}SCAN functional by Furness *et al.*[84,85] was used in the r^{2}SCAN-3c methodology[86] with a def2-mTZVPP[87] basis set. The geometrical counterpoise correction (gCP) by Kruse and Grimme[88] is part of this methodology as well kruseas Grimme's D4 dispersion[89,90] correction scheme. Calculations including La employ the Def2-ECP (effective core potential)[91] for it and an auxiliary coulomb fitting basis def2/J.[92] Thermochemical quantities were calculated from the analytical frequencies with the default ORCA settings (temperature of 298.15 K and pressure of 1.0 atm). ORCA uses the Quasi-RRHO approach by Grimme[93] to correct issues related to the problematic harmonic approximation for low frequencies. To reduce computational cost and complexity, we limit DFT calculations of these large molecules to Ln = La, as the La^{3+} ion does not have f-electrons and results in a closed shell system, reducing the computational cost by a factor of two compared to open shell systems.

Data availability

The data supporting this article have been included as part of the ESI.† Crystallographic data for compound H_8L^2 and Yb complex **6** has been deposited at the CCDC under CCDC-2384275 and CCDC-2384276.† DFT: the full workflow including all scripts, plots, inputs, and outputs generated in this project are available on Zenodo, **https://zenodo.org/**. P. Melix, Luminescent Lathanide Complexes supported by Macrocyclic Schiff-base/calix[4]arene-ligands: synthesis, Structures, and Luminescence properties, 2023.

Conflicts of interest

There are no conflicts to declare.

Acknowledgements

We are grateful to Prof. Dr H. Krautscheid for providing facilities for X-ray crystallographic measurements. We would like to thank Christopher Fischer for assistance in the synthesis of compounds. This work was supported by the University of Leipzig and by the Federal Ministry for Education and Research (BMBF) under grant number 02NUK014C. This work was funded in part by the German Research Foundation (DFG) within the CRC Transregio TRR 386 – B1 (514664767). We also thank the DFG for an FTIR spectrometer (Project number 448298270). Computations for this work were done (in part) using resources of the Leipzig University Computing Center.

References

1 J.-C. G. Bünzli and C. Piguet, Taking Advantage of Luminescent Lanthanide Ions, *Chem. Soc. Rev.*, 2005, **34**(12), 1048–1077.
2 C. Piguet and J.-C. G. Bünzli, Mono-and Polymetallic Lanthanide-Containing Functional Assemblies: A Field between Tradition and Novelty, *Chem. Soc. Rev.*, 1999, **28**(6), 347–358.
3 A. M. Nonat and L. J. Charbonnière, Upconversion of Light with Molecular and Supramolecular Lanthanide Complexes, *Coord. Chem. Rev.*, 2020, **409**, 213192, DOI: 10.1016/j.ccr.2020.213192.
4 A. E. V. Gorden, J. Xu, K. N. Raymond and P. Durbin, Rational Design of Sequestering Agents for Plutonium and Other Actinides, *Chem. Rev.*, 2003, **103**(11), 4207–4282, DOI: 10.1021/cr990114x.
5 S. J. Butler and D. Parker, Anion Binding in Water at Lanthanide Centres: From Structure and Selectivity to Signalling and Sensing, *Chem. Soc. Rev.*, 2013, **42**(4), 1652–1666, DOI: 10.1039/C2CS35144G.
6 M. L. Aulsebrook, B. Graham, M. R. Grace and K. L. Tuck, Lanthanide Complexes for Luminescence-Based Sensing of Low Molecular Weight Analytes, *Coord. Chem. Rev.*, 2018, **375**, 191–220, DOI: 10.1016/j.ccr.2017.11.018.
7 L. Abad Galán, D. Aguilà, Y. Guyot, V. Velasco, O. Roubeau, S. J. Teat, M. Massi and G. Aromí, Accessing Lanthanide-to-Lanthanide Energy Transfer in a Family of Site-Resolved [LnIIILnIII′] Heterodimetallic Complexes, *Chem. – Eur. J.*, 2021, **27**(25), 7288–7299, DOI: 10.1002/chem.202005327.
8 L. Abad Galán, A. N. Sobolev, B. W. Skelton, E. Zysman-Colman, M. I. Ogden and M. Massi, Energy Transfer between Eu^{3+} and Nd^{3+} in Near-Infrared Emitting β-Triketonate Coordination Polymers, *Dalton Trans.*, 2018, **47**(35), 12345–12352, DOI: 10.1039/C8DT02499E.
9 L. Zhou, P. A. Tanner, W. Zhou, Y. Ai, L. Ning, M. M. Wu and H. Liang, Unique Spectral Overlap and Resonant Energy Transfer between Europium(II) and Ytterbium(III) Cations: No Quantum Cutting, *Angew. Chem., Int. Ed.*, 2017, **56**(35), 10357–10361, DOI: 10.1002/anie.201703331.
10 A. Nonat, S. Bahamyirou, A. Lecointre, F. Przybilla, Y. Mély, C. Platas-Iglesias, F. Camerel, O. Jeannin and L. J. Charbonnière, Molecular Upconversion in Water in Heteropolynuclear Supramolecular Tb/Yb Assemblies, *J. Am. Chem. Soc.*, 2019, **141**(4), 1568–1576, DOI: 10.1021/jacs.8b10932.
11 H. Yao, G. Calvez, C. Daiguebonne, K. Bernot, Y. Suffren and O. Guillou, Hetero-Hexalanthanide Complexes: A New Synthetic Strategy for Molecular Thermometric Probes, *Inorg. Chem.*, 2019, **58**(23), 16180–16193, DOI: 10.1021/acs.inorgchem.9b02668.
12 T. J. Sørensen and S. Faulkner, Multimetallic Lanthanide Complexes: Using Kinetic Control To Define Complex Multimetallic Arrays, *Acc. Chem. Res.*, 2018, **51**(10), 2493–2501, DOI: 10.1021/acs.accounts.8b00205.
13 D. Maniaki, A. Sickinger, L. A. Barrios, D. Aguilà, O. Roubeau, Y. Guyot, F. Riobé, O. Maury, L. Abad Galán and G. Aromí, Energy Exchange between Nd^{3+} and Er^{3+} Centers within Molecular Complexes, *Chem. Sci.*, 2024, **15**(44), 18295–18302, DOI: 10.1039/D4SC03994G.
14 M. E. Thornton, J. Hemsworth, S. Hay, P. Parkinson, S. Faulkner and L. S. Natrajan, Heterometallic Lanthanide Complexes with Site-Specific Binding That Enable Simultaneous Visible and NIR-Emission, *Front. Chem.*, 2023, 11.
15 F. Artizzu, L. Pilia, A. Serpe, D. Mara, M. F. Casula, L. Marchiò and P. Deplano, Anion-Induced Structural Diversity and Optical Chromism in a Series of Cyano-Bridged Heterometallic 3d–4f Coordination Polymers, *Molecules*, 2023, **28**(6), 2871.
16 F. Artizzu, F. Quochi, A. Serpe, E. Sessini and P. Deplano, Tailoring Functionality through Synthetic Strategy in Heterolanthanide Assemblies, *Inorg. Chem. Front.*, 2015, **2**(3), 213–222.
17 Y. Luo, G. Calvez, S. Freslon, K. Bernot, C. Daiguebonne and O. Guillou, Lanthanide Aminoisophthalate Coordination Polymers: A Promising System for Tunable Luminescent Properties, *Eur. J. Inorg. Chem.*, 2011, (25), 3705–3716, DOI: 10.1002/ejic.201100437.
18 S. Freslon, Y. Luo, C. Daiguebonne, G. Calvez, K. Bernot and O. Guillou, Brightness and Color Tuning in a Series of Lanthanide-Based Coordination Polymers with Benzene-1,2,4,5-Tetracarboxylic Acid as a Ligand, *Inorg. Chem.*, 2016, **55**(2), 794–802.
19 X. Fan, S. Freslon, C. Daiguebonne, G. Calvez, L. Le Pollès, K. Bernot and O. Guillou, Heteronuclear Lanthanide-Based Coordination Polymers Exhibiting Tunable Multiple Emission Spectra, *J. Mater. Chem. C*, 2014, **2**(28), 5510–5525.
20 S. Freslon, Y. Luo, G. Calvez, C. Daiguebonne, O. Guillou, K. Bernot, V. Michel and X. Fan, Influence of Photoinduced Electron Transfer on Lanthanide-Based Coordination Polymer Luminescence: A Comparison between Two Pseudoisoreticular Molecular Networks, *Inorg. Chem.*, 2014, **53**(2), 1217–1228.
21 X. Zhou, L. Chen, Z. Feng, S. Jiang, J. Lin, Y. Pang, L. Li and G. Xiang, Color Tunable Emission and Low-Temperature Luminescent Sensing of Europium and Terbium Carboxylic Acid Complexes, *Inorg. Chim. Acta*, 2018, **469**, 576–582.
22 E. Bartolomé, J. Bartolomé, A. Arauzo, J. Luzón, R. Cases, S. Fuertes, V. Sicilia, A. I. Sanchez-Cano, J. Aporta and S. Melnic, Heteronuclear {Tb x Eu 1−X} Furoate 1D Polymers Presenting Luminescent Properties and SMM Behavior, *J. Mater. Chem. C*, 2018, **6**(19), 5286–5299.
23 Z. V. Dobrokhotova, S. P. Petrosyants, A. B. Ilyukhin, Y. S. Zavorotny, V. I. Gerasimova, Y. A. Mikhlina, N. N. Efimov and V. M. Novotortsev, New Neutral and Anionic Thiocyanate Complexes of Y(III) and Eu(III) with 2,2′-Bipyridine and 1,10-Phenanthroline: Synthesis, Structures, Thermal Behavior and Photophysical Properties, *Inorg. Chim. Acta*, 2017, **456**, 76–85.
24 I. G. Fomina, Z. V. Dobrokhotova, A. B. Ilyukhin, V. I. Zhilov, A. S. Bogomyakov, A. A. Antoshkov, Y. S. Zavorotny, V. I. Gerasimova, V. M. Novotortsev and I. L. Eremenko, Heterodinuclear (Sm, Tb) Lanthanide Pivalates with Heterocyclic N-Donors: Synthesis, Structure, Thermal Behavior,

and Magnetic and Photoluminescence Properties, *Dalton Trans.*, 2014, **43**(48), 18104–18116.

25 Y. C. Miranda, L. L. A. L. Pereira, J. H. P. Barbosa, H. F. Brito, M. C. F. C. Felinto, O. L. Malta, W. M. Faustino and E. E. S. Teotonio, The Role of the Ligand-to-Metal Charge-Transfer State in the Dipivaloylmethanate-Lanthanide Intramolecular Energy Transfer Process, *Eur. J. Inorg. Chem.*, 2015, (18), 3019–3027.

26 Q. Li, T. Li and J. Wu, Luminescence of Europium (III) and Terbium (III) Complexes Incorporated in Poly (Vinyl Pyrrolidone) Matrix, *J. Phys. Chem. B*, 2001, **105**(49), 12293–12296.

27 D. T. de Lill, A. de Bettencourt-Dias and C. L. Cahill, Exploring Lanthanide Luminescence in Metal–Organic Frameworks: Synthesis, Structure, and Guest-Sensitized Luminescence of a Mixed Europium/Terbium-Adipate Framework and a Terbium-Adipate Framework, *Inorg. Chem.*, 2007, **46**(10), 3960–3965.

28 I. G. Fomina, Z. V. Dobrokhotova, G. G. Aleksandrov, V. I. Zhilov, I. P. Malkerova, A. S. Alikhanyan, D. M. Zhigunov, A. S. Bogomyakov, V. I. Gerasimova and V. M. Novotortsev, Synthesis and Characterization of New Heterodinuclear (Eu, Tb) Lanthanide Pivalates, *Polyhedron*, 2013, **50**(1), 297–305.

29 E. Chelebaeva, J. Long, J. Larionova, R. A. S. Ferreira, L. D. Carlos, F. A. Almeida Paz, J. B. R. Gomes, A. Trifonov, C. Guérin and Y. Guari, Bifunctional Mixed-Lanthanide Cyano-Bridged Coordination Polymers $Ln(0.5)Ln'(0.5)(H_2O)_5$ $[W(CN)_8]$(Ln/Ln′ = Eu^{3+}/Tb^{3+}, Eu^{3+}/Gd^{3+}, Tb^{3+}/Sm^{3+}), *Inorg. Chem.*, 2012, **51**(16), 9005–9016.

30 E. F. Schubert, *Light-Emitting Diodes*, Cambridge University Press, 2018.

31 J.-C. G. Bünzli and S. V. Eliseeva, Basics of Lanthanide Photophysics, *Lanthanide Luminescence*, 2010, pp. 1–45, DOI: 10.1007/4243_2010_3.

32 D. Gutsche, *Calixarenes: An Introduction*, RSC Publishing, Cambridge, 2nd edn, 2008, DOI: 10.1039/9781847558190.

33 V. Böhmer, Calixarenes, Macrocycles with (Almost) Unlimited Possibilities, *Angew. Chem., Int. Ed. Engl.*, 1995, **34**(7), 713–745, DOI: 10.1002/anie.199507131.

34 L. Baldini, F. Sansone, A. Casnati and R. Ungaro, Calixarenes in Molecular Recognition, in *Supramolecular Chemistry, From Molecules to nanometerials*, ed. J. W. Steed and P. A. Gale, John-Wiley & Sons Ltd, Hoboken, USA, 2012, pp. 863–894.

35 D. Sémeril and D. Matt, Synthesis and Catalytic Relevance of P(III) and P(V)-Functionalised Calixarenes and Resorcinarenes, *Coord. Chem. Rev.*, 2014, **279**, 58–95.

36 C. Redshaw, Coordination Chemistry of the Larger Calixarenes, *Coord. Chem. Rev.*, 2003, **244**(1–2), 45–70.

37 P. D. Beer and E. J. Hayes, Transition Metal and Organometallic Anion Complexation Agents, *Coord. Chem. Rev.*, 2003, **240**(1–2), 167–189.

38 B. M. Furphy, J. M. Harrowfield, D. L. Kepert, B. W. Skelton, A. H. White and F. R. Wilner, Bimetallic Lanthanide Complexes of the Calixarenes: Europium(III) and tert-Butylcalix[8]arene, *Inorg. Chem.*, 1987, **26**, 4231–4236.

39 P. D. Beer, M. G. B. Drew, M. Kan, P. B. Leeson, M. I. Ogden and G. Williams, Lanthanide Structures, Coordination, and Extraction Investigations of a 1,3-Bis (Diethyl Amide)-Substituted Calix [4] Arene Ligand, *Inorg. Chem.*, 1996, **35**(8), 2202–2211.

40 A. Casnati, L. Baldini, F. Sansone, R. Ungaro, N. Armaroli, D. Pompei and F. Barigelletti, Synthesis, Complexation and Photophysics in Protic Solvents of Lanthanide Complexes of Novel Calix [4] Arene Polycarboxylic-2,2′-Bipyridine Mixed Ligands, *Supramol. Chem.*, 2002, **14**(2–3), 281–289.

41 G. Guillemot, B. Castellano, T. Prangé, E. Solari and C. Floriani, Use of Calix [4] Arenes in the Redox Chemistry of Lanthanides: The Reduction of Dinitrogen by a Calix [4] Arene–Samarium Complex, *Inorg. Chem.*, 2007, **46**(13), 5152–5154.

42 G. B. Deacon, M. G. Gardiner, P. C. Junk, J. P. Townley and J. Wang, Rare-Earth Metalation of Calix [4] Pyrrole/Calix [4] Arene Free of Alkali–Metal Companions, *Organometallics*, 2012, **31**(10), 3857–3864.

43 N. Sabbatini, M. Guardigli, A. Mecati, V. Balzani, R. Ungaro, E. Ghidini, A. Casnati and A. Pochini, Encapsulation of Lanthanide Ions in Calixarene Receptors. A Strongly Luminescent Terbium (3+) Complex, *J. Chem. Soc. Chem. Commun.*, 1990, (12), 878–879.

44 N. Sato and S. Shinkai, Energy-Transfer Luminescence of Lanthanide Ions Encapsulated in Sensitizer-Modified Calix [4] Arenes, *J. Chem. Soc., Perkin Trans. 2*, 1993, (4), 621–624.

45 F. J. Steemers, W. Verboom, D. N. Reinhoudt, E. B. van der Tol and J. W. Verhoeven, New Sensitizer-Modified Calix [4] Arenes Enabling near-UV Excitation of Complexed Luminescent Lanthanide Ions, *J. Am. Chem. Soc.*, 1995, **117**(37), 9408–9414.

46 B. W. Ennis, S. Muzzioli, B. L. Reid, D. M. D'Alessio, S. Stagni, D. H. Brown, M. I. Ogden and M. Massi, Recyclable Calix [4] Arene–Lanthanoid Luminescent Hybrid Materials with Color-Tuning and Color-Switching Properties, *Dalton Trans.*, 2013, **42**(19), 6894–6901.

47 D. D'Alessio, S. Muzzioli, B. W. Skelton, S. Stagni, M. Massi and M. I. Ogden, Luminescent Lanthanoid Complexes of a Tetrazole-Functionalised Calix[4]Arene, *Dalton Trans.*, 2012, **41**(16), 4736–4739.

48 M. Massi and M. I. Ogden, Luminescent Lanthanoid Calixarene Complexes and Materials, *Materials*, 2017, **10**(12), 1369.

49 S. Ullmann, P. Hahn, P. Mini, K. L. Tuck, A. Kahnt, B. Abel, M. E. G. Suburu, C. A. Strassert and B. Kersting, Mixed-Ligand Lanthanide Complexes Supported by Ditopic Bis (Imino-Methyl)-Phenol/Calix[4]Arene Macrocycles: Synthesis, Structures, and Luminescence Properties of $[Ln2(L^2)(MeOH)_2]$(Ln = La, Eu, Tb, Yb), *Dalton Trans.*, 2020, **49**(32), 11179–11191.

50 S. Dasari and A. K. Patra, Luminescent Europium and Terbium Complexes of Dipyridoquinoxaline and Dipyridophenazine Ligands as Photosensitizing Antennae: Structures and Biological Perspectives, *Dalton Trans.*, 2015, **44**(46), 19844–19855.

51 J. K. Molloy, C. Philouze, L. Fedele, D. Imbert, O. Jarjayes and F. Thomas, Seven-Coordinate Lanthanide Complexes with a Tripodal Redox Active Ligand: Structural, Electrochemical and Spectroscopic Investigations, *Dalton Trans.*, 2018, **47**(31), 10742–10751.

52 W.-C. Zhang and Z.-T. Huang, Synthesis of 4-*Tert*-Butylcalix[4]Arenes Bearing Two Schiff-Base Units at the Lower Rim, *Synthesis*, 1997, 1073–1076.

53 X. Wu, P. Zhang, Z. Yang, S. Zhang, H. Liu, W. Chi, X. Li, Y. Dong, N. Qiu and L. Yan, Polymerization of Phenylacetylenes by Binuclear Rhodium Catalysts with Different Para-Binucleating Phenoxyiminato Linkages, *Polym. Chem.*, 2019, **10**(30), 4163–4172.

54 A. Arduini, A. Pochini, S. Raverberi and R. Ungaro, P-*t*-Butyl-Calix[4]Arene Tetracarboxylic Acid. A Water Soluble Calixarene in a Cone Structure, *J. Chem. Soc., Chem. Commun.*, 1984, (15), 981–982.

55 M. Hesse, H. Meier and B. Zeeh, *Spektroskopische Methoden in Der Organischen Chemie*, Thieme, 2005.

56 B. Schneider, J. Štokr, P. Schmidt, M. Mihailov, S. Dirlikov and N. Peeva, Stretching and Deformation Vibrations of CH_2, $C(CH_3)$ and $O(CH_3)$ Groups of Poly(Methyl Methacrylate), *Polymer*, 1979, **20**(6), 705–712.

57 G. Kortüm and D. Oelkrug, Über Den Streukoeffizienten der Kubelka-Munk-Theorie, *Z. Naturforsch., A*, 1964, **19**(1), 28–37.

58 M. Israr, F. Faheem, F. T. Minhas, A. Rauf, S. Rauf, M. R. Shah, F. Rahim, K. Shah and M. I. Bhanger, Extraction Properties of Calix[4]Arenes towards Sulphonated Dyes, *Am. J. Analyt. Chem.*, 2016, **7**(2), 219–232.

59 A. Pietropaolo, C. Cozza, Z. Zhang and T. Nakano, Temperature-Dependent UV Absorption of Biphenyl Based on Intra-Molecular Rotation Investigated within a Combined Experimental and TD-DFT Approach, *Liq. Cryst.*, 2018, **45**(13–15), 2048–2053, DOI: **10.1080/02678292.2018.1501108**.

60 S. Ullmann, R. Schnorr, C. Laube, B. Abel and B. Kersting, Photoluminescence Properties of Tetrahedral Zinc(II) Complexes Supported by Calix[4]Arene-Based Salicylaldiminato Ligands, *Dalton Trans.*, 2018, **47**(16), 5801–5811, DOI: **10.1039/C8DT00757H**.

61 B. Landeros-Rivera and J. Hernández-Trujillo, Control of Molecular Conformation and Crystal Packing of Biphenyl Derivatives, *ChemPlusChem*, 2022, **87**(1), e202100492, DOI: **10.1002/cplu.202100492**.

62 A. W. Coleman, S. G. Bott, S. D. Morley, C. M. Means, K. D. Robinson, H. Zhang and J. L. Atwood, Novel Layer Structure of Sodium Calix[4]Arenesulfonate Complexes—a Class of Organic Clay Mimics, *Angew. Chem., Int. Ed. Engl.*, 1988, **27**(10), 1361–1362.

63 M. Makha, A. N. Sobolev and C. L. Raston, Non-Covalent Expansion of an Organic Bilayer Involving Exo-Cavity Interplay of Tetraphenylphosphonium with Para-Sulfonato-Calix [4] Arene, *Chem. Commun.*, 2006, (1), 57–59.

64 M. Pinsky and D. Avnir, Continuous Symmetry Measures. 5. The Classical Polyhedra, *Inorg. Chem.*, 1998, **37**(21), 5575–5582.

65 M. Pinsky, C. Dryzun, D. Casanova, P. Alemany and D. Avnir, Analytical Methods for Calculating Continuous Symmetry Measures and the Chirality Measure, *J. Comput. Chem.*, 2008, **29**(16), 2712–2721, DOI: **10.1002/jcc.20990**.

66 P. Hahn, S. Ullmann, A. Kahnt, B. Abel and B. Kersting, Synthesis, Structures and Luminescence Properties of Dinuclear Nd, Eu, Tb, and Yb Complexes Supported by a Pendant Picolyl-Imine Calix[4]Arene Ligand, *Inorg. Chim. Acta*, 2021, **514**, 119983, DOI: **10.1016/j.ica.2020.119983**.

67 H. C. Aspinall, *F-Block Chemistry; Oxford chemistry primers*, Oxford University Press, 2020.

68 A. F. Holleman, in *Lehrbuch Der Anorganischen Chemie*, ed. E. Wiberg, de Gruyter, 102nd edn, 2007.

69 K. Binnemans, Interpretation of Europium(III) Spectra, *Coord. Chem. Rev.*, 2015, **295**, 1–45, DOI: **10.1016/j.ccr.2015.02.015**.

70 P. P. Ferreira da Rosa, Y. Kitagawa and Y. Hasegawa, Luminescent Lanthanide Complex with Seven-Coordination Geometry, *Coord. Chem. Rev.*, 2020, **406**, 213153, DOI: **10.1016/j.ccr.2019.213153**.

71 M. Latva, H. Takalo, V.-M. Mukkala, C. Matachescu, J. C. Rodríguez-Ubis and J. Kankare, Correlation between the Lowest Triplet State Energy Level of the Ligand and Lanthanide(III) Luminescence Quantum Yield, *J. Lumin.*, 1997, **75**(2), 149–169, DOI: **10.1016/S0022-2313(97)00113-0**.

72 W. Ngeontae, W. Janrungroatsakul, N. Morakot, W. Aeungmaitrepirom and T. Tuntulani, New Silver Selective Electrode Fabricated from Benzothiazole Calix [4] Arene: Speciation Analysis of Silver Nanoparticles, *Sens. Actuators, B*, 2008, **134**(2), 377–385.

73 H. Halouani, I. Dumazet-Bonnamour, M. Perrin and R. Lamartine, First Synthesis and Structure of β-Ketoimine Calix[4]Arenes: Complexation and Extraction Studies, *J. Org. Chem.*, 2004, **69**(20), 6521–6527.

74 Stoe & Cie, STOE & Cie GmbH-AREA and X-RED 32; V2.4. 2.1, Darmstadt, Germany, 2024.

75 G. M. Sheldrick, SHELXT–Integrated Space-Group and Crystal-Structure Determination, *Acta Crystallogr., Sect. A: Found. Adv.*, 2015, **71**(1), 3–8.

76 O. V. Dolomanov, L. J. Bourhis, R. J. Gildea, J. A. K. Howard and H. Puschmann, OLEX2: A Complete Structure Solution, Refinement and Analysis Program, *J. Appl. Crystallogr.*, 2009, **42**(2), 339–341.

77 PLAMS, SCM, Theoretical Chemistry, Vrije Universiteit, Amsterdam, The Netherlands, 2024, **https://github.com/SCM-NV/PLAMS**.

78 A. Hjorth Larsen, J. Jørgen Mortensen, J. Blomqvist, I. E. Castelli, R. Christensen, M. Dułak, J. Friis, M. N. Groves, B. Hammer, C. Hargus, E. D. Hermes, P. C. Jennings, P. Bjerre Jensen, J. Kermode, J. R. Kitchin, E. Leonhard Kolsbjerg, J. Kubal, K. Kaasbjerg, S. Lysgaard, J. Bergmann Maronsson, T. Maxson, T. Olsen, L. Pastewka, A. Peterson, C. Rostgaard, J. Schiøtz, O. Schütt, M. Strange, K. S. Thygesen, T. Vegge, L. Vilhelmsen, M. Walter, Z. Zeng and K. W. Jacobsen, The Atomic Simulation Environment—a Python Library for Working with Atoms, *J. Phys.: Condens.*

Matter, 2017, **29**(27), 273002, DOI: 10.1088/1361-648X/aa680e.

79 J. D. Hunter, Matplotlib: A 2D Graphics Environment, *Comput. Sci. Eng.*, 2007, **9**(3), 90–95, DOI: 10.1109/MCSE.2007.55.

80 W. Humphrey, A. Dalke and K. Schulten, VMD: Visual Molecular Dynamics, *J. Mol. Graphics*, 1996, **14**(1), 33–38, DOI: 10.1016/0263-7855(96)00018-5.

81 P. Melix, *Luminescent Lathanide Complexes Supported by Macrocyclic Schiff-Base/Calix[4]Arene-Ligands: Synthesis, Structures, and Luminescence Properties*, 2023, DOI: 10.5281/zenodo.8116993.

82 F. Neese, The ORCA Program System, *Wiley Interdiscip. Rev.: Comput. Mol. Sci.*, 2012, **2**(1), 73–78, DOI: 10.1002/wcms.81.

83 F. Neese, Software Update: The ORCA Program System, Version 4.0, *Wiley Interdiscip. Rev.: Comput. Mol. Sci.*, 2018, **8**(1), e1327, DOI: 10.1002/wcms.1327.

84 J. W. Furness, A. D. Kaplan, J. Ning, J. P. Perdew and J. Sun, Accurate and Numerically Efficient R2SCAN Meta-Generalized Gradient Approximation, *J. Phys. Chem. Lett.*, 2020, **11**(19), 8208–8215, DOI: 10.1021/acs.jpclett.0c02405.

85 J. W. Furness, A. D. Kaplan, J. Ning, J. P. Perdew and J. Sun, Correction to Accurate and Numerically Efficient R2SCAN Meta-Generalized Gradient Approximation, *J. Phys. Chem. Lett.*, 2020, **11**(21), 9248, DOI: 10.1021/acs.jpclett.0c03077.

86 S. Grimme, A. Hansen, S. Ehlert and J. M. Mewes, R(2)SCAN-3c: A "Swiss Army Knife" Composite Electronic-Structure Method, *J. Chem. Phys.*, 2021, **154**(6), 64103, DOI: 10.1063/5.0040021.

87 J. G. Brandenburg, C. Bannwarth, A. Hansen and S. Grimme, B97-3c: A Revised Low-Cost Variant of the B97-D Density Functional Method, *J. Chem. Phys.*, 2018, **148**(6), 064104.

88 H. Kruse and S. Grimme, A Geometrical Correction for the Inter- and Intra-Molecular Basis Set Superposition Error in Hartree-Fock and Density Functional Theory Calculations for Large Systems, *J. Chem. Phys.*, 2012, **136**(15), 154101, DOI: 10.1063/1.3700154.

89 E. Caldeweyher, C. Bannwarth and S. Grimme, Extension of the D3 Dispersion Coefficient Model, *J. Chem. Phys.*, 2017, **147**(3), 034112, DOI: 10.1063/1.4993215.

90 E. Caldeweyher, S. Ehlert, A. Hansen, H. Neugebauer, S. Spicher, C. Bannwarth and S. Grimme, A Generally Applicable Atomic-Charge Dependent London Dispersion Correction, *J. Chem. Phys.*, 2019, **150**(15), 154122, DOI: 10.1063/1.5090222.

91 D. Andrae, U. Häußermann, M. Dolg, H. Stoll and H. Preuß, Energy-Adjustedab Initio Pseudopotentials for the Second and Third Row Transition Elements, *Theor. Chim. Acta*, 1990, **77**(2), 123–141, DOI: 10.1007/BF01114537.

92 F. Weigend, Accurate Coulomb-Fitting Basis Sets for H to Rn, *Phys. Chem. Chem. Phys.*, 2006, **8**(9), 1057–1065, DOI: 10.1039/B515623H.

93 S. Grimme, Supramolecular Binding Thermodynamics by Dispersion-Corrected Density Functional Theory, *Chem. – Eur. J.*, 2012, **18**(32), 9955–9964, DOI: 10.1002/chem.201200497.

